RESEARCH PAPER

Enhanced Ionic Conductivity in PVA Based Solid Polymer Films Blended with KCl Nanoparticles: Thermal, Vibrational, Morphological and Electrical Insights

*Ahmed Almzainy, Kamel Said *, Mahdi Hdidar, Mourad Arous*

Laboratory of Ceramic Composites and Polymer Materials (LaMaCoP), Faculty of Sciences of Sfax, University of Sfax, Tunisia

ARTICLE INFO

Article History:
Received 09 August 2026
Accepted 10 October 2026
Published 01 January 2027

Keywords:
Biodegradable
Ionic conductivity
Hygroscopicity
KCl nanoparticles
PVA based solid polymer film
Sustainable

ABSTRACT

Sustainable biodegradable solid blend polymer films based on polyvinyl alcohol (PVA) doped with various weight fractions (from 3.6 to 42.7 %) of potassium chloride (KCl) nanoparticles were developed via the solution casting method. Differential Scanning Calorimetry revealed that KCl contents above 10.1 % significantly reduce crystallinity, while water evaporation exhibits overlapping peaks. Fourier Transform Infrared spectroscopy confirmed the interactions between PVA and the KCl nanoparticles. Scanning Electron Microscopy combined with Energy Dispersive X-ray mapping highlighted the formation of hydrated KCl crystals at dopant levels above 10.1 %. Broadband Dielectric Spectroscopy revealed that the AC conductivity is strongly dependent on KCl content, frequency (10^{-1} to 10^{6} Hz), and temperature (20 to 150°C), with the DC conductivity extracted from the low-frequency plateau exhibiting Arrhenius behavior. DC conductivity increases with KCl content up to 10.1 %, reaching $2.5x10^{-7}$ S/cm at 20 °C, representing a five order of magnitude enhancement over pure PVA. The interesting correlations between thermal, vibrational, morphological, and electrical properties demonstrate that 6.9 to 10.1 % of KCl nanoparticles blending effectively enhances ionic conduction in PVA based solid polymer films, offering promising perspectives for flexible electronics, sensors and energy storage applications.

How to cite this article
Almzainy A., Said K., Hdidar M., Arous M. Enhanced Ionic Conductivity in PVA Based Solid Polymer Films Blended with KCl Nanoparticles: Thermal, Vibrational, Morphological and Electrical Insights. J Nanostruct, 2027; 17(1):75-94. DOI: 10.22052/JNS.2027.01.008

INTRODUCTION

Actually, interest in biodegradable polymer-based solid films with distinctive electrical, thermal and mechanical properties has intensified due to the emergence of sustainable energy storage systems. The growing use of polymer-based solid films in a wide range of technological applications is mainly driven by their improved safety, mechanical flexibility, reusability and applicability. Moreover, advances in polymer-based solid films play a pivotal role in driving scientific progress and underpin vital improvement in fields such as solar energy, light-emitting diodes, sensors, laser systems, pacemaker batteries, and many other sectors [1–6]. However, environmental concerns, non-biodegradability, toxicity, and the reliance

* *Corresponding Author Email: kamel.said@fss.usf.tn*

This work is licensed under the Creative Commons Attribution 4.0 International License.
To view a copy of this license, visit http://creativecommons.org/licenses/by/4.0/.

on petroleum-based plastic have prompted the search for sustainable biodegradable polymer-based solid films.

Polyvinyl alcohol (PVA) stands out as one of the most extensively studied sustainable biopolymer-based solid films, due to its distinctive electrical, optical, mechanical, and safety properties, as well as its wide applicability. Indeed, PVA is commonly employed as a solid polymer electrolyte in fuel cells, high-energy rechargeable batteries, supercapacitors, and other industrial applications [7–12]. It is recognized for its superior electrical insulation, high charge storage capacity [7], exceptional tensile strength, and excellent film-forming ability, which provides high elasticity and quality, making it indispensable for coating applications that enhance product longevity [8]. Additionally, PVA is biocompatible, transparent, biodegradable, and easy to process, allowing for the casting of materials with controlled thickness. Its polar hydroxyl (–OH) groups facilitate dissolution in water and various organic solvents, making it a versatile biomaterial for medical and pharmaceutical applications [13–16]. These hydroxyl groups also enable hydrogen bonding, allowing PVA to readily incorporate and dissolve added ions (polymer blending) by forming weak electrostatic interactions with dissociated cations and anions. Ultimately, the number of free ions increases with increasing ion concentration, thereby enhancing ionic conductivity at both room and operational temperatures, a desirable feature for several applications [17,18]. Therefore, blending or doping PVA with various elements provides an effective strategy for tailoring its properties, thereby achieving enhanced functionality for specific applications. In this framework, potassium chloride (KCl) nanoparticles were selected as dopant in this work to boost functionality of PVA based solid film. Indeed, KCl has widespread industrial and scientific applications. It is commonly used in food processing, fertilizers, and pharmaceuticals [19], as well as in water treatment, natural gas, and petroleum extraction as a completion fluid. In optics, KCl serves as a material for infrared spectroscopy and high-power CO_2 laser systems due to its excellent optical transparency. In the field of large-scale energy storage batteries, potassium ions (K^+) are emerging as a viable alternative to lithium due to their natural abundance, lower cost, and comparable electrochemical performance [20]. Additionally, the mechanical softness of KCl salt facilitates effective and stable contact with other battery components. Moreover, potassium chloride exhibits significant hygroscopic properties, allowing it to absorb and retain moisture from the environment. The combination of its hygroscopic nature and its ability to interact with organic compounds is also relevant in the context of biomass burning aerosol particles [21,22].

This work aims to combine the high ability of KCl salt to enhance ionic conductivity with its strong hygroscopic nature to develop PVA-based solid films blended with various weight fractions of KCl nanoparticles. The objective is to improve their ionic conductivity for use in numerous technological and industrial applications. Furthermore, the temperature dependence of this conductivity was examined in the range of 20 – 150°C, since the operating temperatures of many practical devices exceed room temperature. To the best of our knowledge, only two previous studies have investigated the ionic conductivity of PVA/KCl solid films. The first study, conducted solely at room temperature using three KCl concentrations (5, 10 and 50%), showed that adding 5% salt enhances ionic conductivity by one order of magnitude at a frequency of 10^6 Hz, whereas a further increase in salt concentration reduces it [23]. The second study investigated lower KCl concentrations (5, 10, and 15%) across a temperature range of 30 – 100°C [24]. Those authors reported that ionic conductivity increases with both dopant concentration and temperature, for instance, adding 15% KCl enhanced ionic conductivity by approximately one order of magnitude across the entire temperature range. Consequently, the combined effects of KCl nanoparticles concentration and temperature on the ionic conductivity of PVA/KCl solid polymer films require further systematic investigation and clarification. This work addresses these shortcomings by systematically examining the impact of six KCl weight fractions ranging between 3.6 and 42.7% on the thermal, vibrational, morphological, and electrical properties across a temperature range of 20 – 150°C of biodegradable PVA based solid films. Thereby, we open new avenues for a comprehensive exploration into ionic conduction mechanisms and demonstrate a marked improvement in DC conductivity of five orders of magnitude. Additionally, we establish an original, detailed interdisciplinary relationship among

CC BY

these attributes, highlighting how ionic doping concentration, hygroscopicity, ionic dissociation, crystallinity, and water retention influence film conductivity. Ultimately, this study reveals novel insights into conduction processes, defining the optimal composition and temperature ranges for practical applications in flexible electronics and energy storage systems.

MATERIALS AND METHODS

Sample preparation

The solution casting method was used to elaborate pure PVA and PVA/KCl films. The nanometric PVA powder, with a molecular weight ranging from 146 000 to 186 000 g/mol and a hydrolysis degree of 88 %, was purchased from Sigma–Aldrich Company. Aqueous potassium chloride $(KCl)_{aq}$ solution 7.46 % (0.0746 g/ml of KCl crystal) was acquired from UNIMED Laboratory.

Homogeneous PVA solutions were prepared by gradually dissolving 0.5 g of nanometric PVA powder in 25 ml of deionized water. To ensure complete dissolution, the solution was magnetically stirred at 70°C for 30 minutes. Indeed, the strong



Fig. 1. Schematic representation of the synthesis protocol of PVA/KCl films. A specific volume of the KCl nanoparticle solution was added to the aqueous PVA solution. The mixture was stirred magnetically at 70°C for an additional three hours, cast onto a Teflon petri dish and allowed to dry for three days.

Table 1. Designations, compositions, and KCl nanoparticles fraction weight of pure PVA and PVA/KCl films.

Film designations	PVA (weight, g)	KCl (mmol)	KCl fraction weight (%)
Pure PVA	0.5	0	0
PK0.25	0.5	0.25	3.6
PK0.5	0.5	0.5	6.9
PK0.75	0.5	0.75	10.1
PK1	0.5	1	13.0
PK3	0.5	3	30.9
PK5	0.5	5	42.7

CC BY

intra− and intermolecular hydrogen bonds in PVA require high aqueous dissolution temperature [25]. At the same time, the aqueous potassium chloride nanoparticles solution was stirred using ultrasonic bath. Next, a specific volume of the KCl solution was measured using a graduated pipette and added to the PVA solution. The mixture was stirred magnetically at 70°C for an additional three hours. The low−viscosity and uniform PVA/KCl nanoparticle aqueous solutions were then cast onto a Teflon petri dish and allowed to dry at ambient temperature (approximately 20°C) for three days. Finally, uniform films approximately 0.2 mm thick were ready for characterization. Obviously, a pure PVA film was achieved by directly drying their aqueous solution. A schematic view of the synthesis protocol of PVA/KCl films is illustrated in Fig. 1. The film's designation, constitution, and KCl fraction weight are detailed in Table 1.

Sample characterization techniques

Differential Scanning Calorimetry (DSC)

This sophisticated technique provides a comprehensive assessment of thermal material properties by measuring the heat flow exchanged during a controlled heating or cooling program. The tested sample (a part of the elaborated film) was first weighed and then sealed in an aluminum pan. It was finally placed in a platinum measuring cell located inside the furnace chamber. The analysis was performed in an adiabatic enclosure to avoid any unwanted heat exchange with the surroundings. The control of the experimental run and the data analysis were achieved using the "Pyris" software program installed on a computer connected to the DSC system. Measurements were performed under a nitrogen atmosphere using a Perkin-Elmer DSC 4000. Over the entire temperature range, the temperature precision was better than 0.1°C.

Fourier Transform Infrared spectroscopy (FT−IR)

This non−destructive technique allows the measurement of the absorption or transmittance of Infrared light by a sample. To this end, a portion of each film was sandwiched between two discs of sodium chloride or potassium chloride. It was scanned in the mid-infrared light (wavenumber range of 4000 – 500 cm^{-1}) with a resolution of 0.5 cm^{-1} using a Perkin Elmer 1000 Spectrometer operating in transmittance mode. The analysis was performed under ambient temperature and atmosphere. The experimental data were recorded on a computer, and a Fourier Transform was applied using the FT−IR software program to obtain the corresponding spectra.

Scanning Electron Microscopy (SEM)

The surface morphology of the films was characterized using a TS Quanta 250 SEM under a high−vacuum environment at room temperature, with a 20 kV beam accelerating voltage and an 800 k magnification scale. The prepared films were fixed to an aluminum stub using adhesive tape and then vacuum − dried for 10 minutes in the SEM chamber. Surface images were performed using the Back Scattered Electron Detector (BSED).

Energy Dispersive X−ray mapping (EDX mapping)

This technique was achieved in combination with scanning electron microscopy. In this fundamental analysis, the surface sample was bombarded with high−energy electrons, which generated the ejection of electrons from the inner K shells of surface atoms. When outer shell electrons (such as those in the L or M shells) drop down to fill these vacancies, the resulting energy differences are emitted as characteristic X−ray photons. A detector collects these X−rays and, through their energy spectra, allows for the identification of the existing elements. Furthermore, by scanning the surface with electrons, color−coded maps were created that highlight the location and distribution of each element. The EDX mapping images reveal imperceptible details in standard SEM images, such as structural information, phase distribution, and surface contamination.

AC Impedance spectroscopy

This non−destructive technique allows the measurement of the real part Z' and imaginary part Z" of the sample impedance Z* at different temperatures and frequencies. For this end, samples were cut from elaborated films into small discs of 10 mm in diameter and sandwiched between two platinum electrodes (20 mm in diameter) under spring pressure to ensure good contact. Measurements were performed from 20 to 150 °C and in a frequency interval from 10^{-1} to 10^{6} Hz, using a Broadband Dielectric Spectrometer (BDS) Novocontrol Alpha Analyzer coupled with a Novocontrol Quatro system temperature controller. The temperature was measured with accuracy greater than 0.2°C. The measuring

CC BY

cell with each sample was sealed in a dry box and kept under a strictly argon atmosphere during the measuring period. Conductivity data were determined from complex impedance measurements using the "Win Data" software program installed on a computer connected to the BDS, which controls the experimental procedure and collects the data.

RESULTS AND DISCUSSION

Thermal properties

The thermal properties of elaborated pure PVA and PVA/KCl films were assessed by DSC analysis. Two heating scans were performed. In the first scan, the sample was heated from -20°C to 150°C at a rate of 5°C/min, followed by a cooling back to -20 °C at the same rate. The second scan, from -20°C to 250°C, was achieved at the same heating rate. The thermograms recorded during both heating scans are presented with the same delay in Fig. 2.

The characteristic temperatures (glass transition temperatures at the first T_{g1} and the second T_{g2} scans, temperature of α–relaxation $T_{\alpha c}$, temperature of melting of the crystalline phase T_m), and the fusion enthalpy ΔH, evaluated using

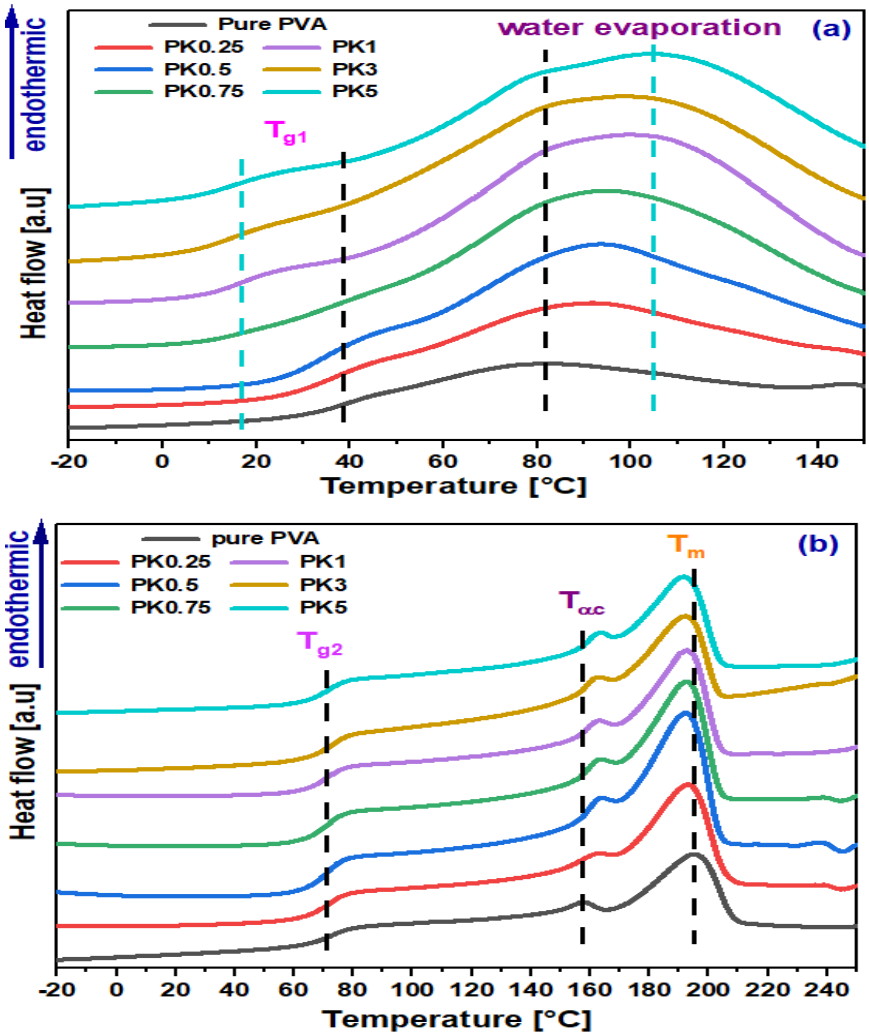


Fig. 2. DSC heating thermograms of pure PVA and PVA/KCl films during the first (a) and second (b) heating scans. The thermograms are presented in order of increasing KCl nanoparticles content from bottom to top (the bottom thermogram corresponds to pure PVA). Dotted lines indicate the positions of characteristic temperatures.

CC BY

the "Pyris" software program, were regrouped in Table 2. The first heating scan (Fig. 2a) displays two thermal phenomena. The first corresponds to a second–order transition attributed to the glass transition, while the second is a first–order transition associated with water evaporation.

The glass transitions

The glass transition temperatures T_g were determined using the midpoint inflexion method. In pure PVA, T_g depends on its molecular weight, degree of hydrolysis, and humidity content [26]. For the first heating scan, T_{g1} ranged from 32.25 to 39.16°C for pure PVA and PVA/KCl films containing less than 13 % KCl, and was approximately 17°C for the others. These values are lower than those measured after water evaporation during the second heating scan, T_{g2} (Table 2). This shift displays the plasticized effect of water. Indeed, water molecules enhance the free volume in the amorphous region, promoting the mobility of PVA chains. Furthermore, the decrease in T_{g1} when the KCl content exceeds 10.1 % (Table 2) indicates an enhanced water plasticization effect, likely associated with the increase of the amorphous fraction.

Water evaporation

The water evaporation process occurs only at the first heating scan, as its characteristic peak is absent in the thermogram of the second scan. The broad peak associated with water evaporation explains that the water molecules undergoing evaporation have a wide distribution of energy states. The thermal evaporation begins with molecules occupying the lowest energy states and then progressively includes more strongly bound molecules as the temperature rises.

As shown in the thermograms of Fig. 2a, the addition of increasing amounts of KCl nanoparticles to PVA induces peak broadening. The broadening towards higher temperatures proves the involvement of additional deeper water states. These additional energetic states are absent in pure PVA; otherwise, they would have undergone evaporation during heating until 150°C. Consequently, the addition of KCl nanoparticles weakens some water bonds, producing an additional energetically deeper state. Another possible effect of this addition is a rearrangement of initial water states, and even the creation of new ones, resulting in the broadening of the water evaporation peaks. Similarly, one can note a variation in the sharpness of water evaporation peaks depending on the KCl content. When the KCl content increases but remains below 13 %, the peak maximum shifts to higher maximum temperatures. This variation indicates that a significant proportion of the evaporated water originates from increasingly strongly bound (deeper) water states, requiring progressively higher temperatures to evaporate. Notably, the peak maximum temperature increases from 82°C (pure PVA) to 92°C (PK0.25) by adding only 3.6 wt % of KCl. This small addition thus induces a perceptible shift toward higher bonding energies for an important portion of the water states undergoing evaporation. This shift grows more slowly with increasing KCl nanoparticles content, with peak maxima at 93.5 and 95°C for PK0.5 and PK0.75, respectively. For the other films, the salient effect is the emergence of two bumps on the water evaporation peaks, which are more discernable for the PK5 film. These bumps likely result from the overlap of two water evaporation peaks associated with two energetically distinct water states. The two peak maxima temperatures are located on either side of the maxima observed at lower KCl content. More precisely, as revealed in the thermogram of PK5 film, these two maxima lie between 82°C (pure PVA) and about 105°C, with higher intensity. The last peak appears to be

Table 2. Characteristic temperatures T_{g1}, T_{g2}, $T_{\alpha c}$, T_m, and fusion enthalpy ΔH of pure PVA and PVA/KCl films, estimated using the "Pyris" software program. The degree of crystallinity χ (%) was calculated as the ratio of ΔH to that of 100 % crystalline PVA.

Samples	T_{g1}(°C)	T_{g2}(°C)	$T_{\alpha c}$(°C)	T_m(°C)	ΔH (J/g)	χ (%)
Pure PVA	39.16	71.31	157.75	194.72	65.60	47.33
PK0.25	37.07	70.63	162.73	193.06	64.39	46.45
PK0.5	36.12	69.84	163.56	192.23	65.23	47.06
PK0.75	32.25	69.14	162.73	192.23	62.37	45.00
PK1	16.58	70.61	162.73	192.64	23.49	16.95
PK3	16.89	71.31	162.73	192.23	16.43	11.85
PK5	17.12	71.52	163.56	191.40	12.92	9.32

CC BY

a continuation of the evaporation peaks displayed at KCl contents below 13 %, while the lower–temperature peak approaches that of pure PVA. These observations highlight a significant change in PVA/KCl films, especially at high KCl nanoparticle contents.

It is important to note that water in PVA has three energetic states [27]. These states generate a continuous energy distribution, as only one water evaporation peak arises in the thermogram of PVA. Although the addition of KCl to PVA is expected to disrupt this configuration, the continuous distribution is preserved, as water evaporation produces either a single peak or the overlap of two peaks (Fig. 2a). A continuous energy distribution of states is typically observed in disordered materials, such as semicrystalline PVA films [28].

It is acknowledged that after drying at room temperature and humidity, the water content in PVA films is approximately 20 %. Even after drying at a higher temperature, PVA quickly returns to its hydrated state. Indeed, PVA chains possess strongly hydrophilic hydroxyl groups serving as the main hydration sites. At low water content, one or two water molecules are bonded to each hydroxyl group. As the water content increases, transition layers form, where the orientations of water molecules are guided by those of previously bonded water molecules, albeit with weaker interactions, followed by bulk water [29]. The strength of water bonding to PVA decreases similarly. Predictably, the removal of water from PVA films undergoes the reverse process, during which PVA chains progressively lose their mobility, leading to crystallization. Concerning the KCl nanoparticles, five water molecules per ion pair (K^+, Cl^-) are needed to dissociate the KCl molecule within a water cluster $[K^+(H_2O)_5Cl^-]$ [30–32]. This first hydrate shell is surrounded by a second one containing 16 to 32 water molecules [33]. The addition of KCl to PVA in aqueous solution breaks some hydrogen bonds between water and the hydroxyl groups of PVA, as new interactions between water molecules and chlorine anions Cl^-. This fact translates to the more hygroscopic nature of KCl. Then, the evaporation of water from the aqueous mixture generates an increasing competition between nanoparticle ions and PVA hydroxyl groups for water molecules. As this process proceeds, the number of hydroxyl groups not bonded to water increases, with a kinetics faster than that observed in the absence of KCl nanoparticles. Simultaneously, since PVA

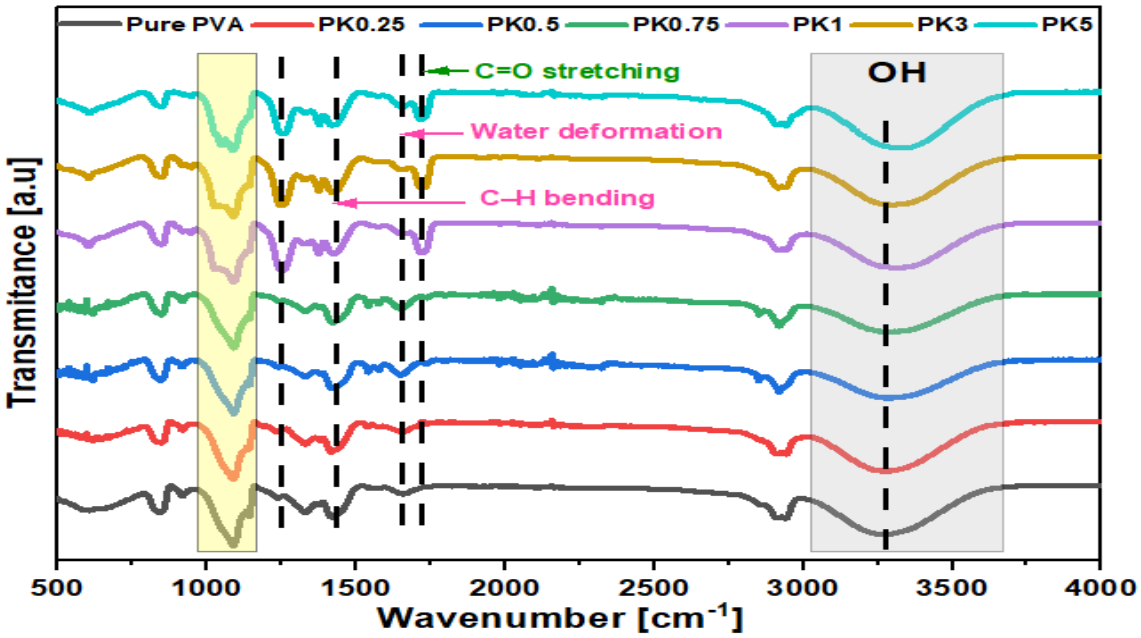


Fig. 3. Normalised FT-IR spectra of pure PVA and PVA/KCl films. The spectra are displayed with a slight offset; in order of increasing KCl nanoparticle content from bottom to top (the first spectrum corresponds to pure PVA). Dotted lines indicate the positions of selected peaks.

(cc) BY

chains still possess sufficient mobility to initiate crystallization, a film with enhanced crystallinity is formed until these chains lose their mobility as the remaining water content becomes too low. After that, the dehydration of K^+ and Cl^- ions begins: several of them become bonded to the hydroxyl groups of PVA, while the others progressively form KCl microcrystals.

α–relaxation and fraction of crystalline region

The thermograms of the second heating scan display two additional peaks above 150°C. The first one, $T_{\alpha c}$, is attributed to α–relaxation occurring at the amorphous – crystalline interface [26,34], while the latter corresponds to the melting of the crystalline phase, T_m. Compared to pure PVA, the addition of KCl nanoparticles induces a slight increase in $T_{\alpha c}$, and a small decrease in T_m (Table 2), which are associated with the effect of KCl on the film nanostructures.

The melting peak enables the evaluation of the fraction of crystalline regions, χ, in the PVA and PVA/KCl films. This fraction (Table 2) is defined as the ratio of the fusion enthalpy ΔH, representing the area of the melting peak divided by the sample weight, to the fusion enthalpy of full crystalline PVA, ΔH_0 = 138.6 J/g [35,36]. It can be noted that this fraction is almost the same for pure PVA, PK0.25, PK0.5, and PK0.75, indicating that the KCl nanoparticles content in these films is too low to induce a significant variation in χ. A drastic decrease in χ is observed for the other films, which is probably attributed to the effect of water. Indeed, it is recognised that water resides in the amorphous regions of the film and deteriorates crystallites at the interface between crystalline and amorphous regions, causing a reduction in the crystalline region [27]. As this decrease in crystallinity is more significant with the addition of KCl nanoparticles and is associated with the emergence of a second water evaporation peak, it is likely that the water involved contains increasing amounts of KCl nanoparticles and is responsible for the decrease in crystallinity. On the other hand, it is also possible that complexes formed through electrostatic interaction between sodium cations K^+ from KCl and the polar groups of PVA chains destroy the crystalline region [37].

FT-IR analysis

FT-IR spectra display characteristic transmittance peaks corresponding to specific vibrational bonds and functional groups [38,39]. To identify modifications in chemical functionalities associated with the addition of KCl nanoparticles to PVA, each FT-IR spectrum was normalized using the "Origin Lab" computer program, scaling the transmittance intensity values to the 0 − 1 range. The normalised FT-IR spectra of PVA and PVA/KCl films are shown, with a slight offset, in Fig. 3. While the spectra present some changes, their main features remain globally the same. This uniformity suggests that the absorption is primarily due to the PVA matrix, although subtle variations in peak shapes indicate the extent of interactions between PVA and the KCl nanoparticles. In the spectra of PVA/KCl films, the position, intensity, width, and shape of all absorption bands may be more or less affected by the amount of KCl nanoparticles added and its hygroscopic behaviour.

Band absorption of the hydroxyl group

The absorption band of the hydroxyl group in PVA film lies between approximately 3026 and 3670 cm^{-1} and is ascribed to the O–H stretching vibration. This vibration is attributed to the intermolecular and intramolecular hydrogen bands between the hydroxyl groups inside the PVA chains [40]. The same absorption band appears in PVA/KCl films within the same wavenumber range, but with a progressive blue shift in shape as the KCl nanoparticles content increases. This wavenumber

Table 3. Wavenumbers of the minima and the extent of the shift of the hydroxyl absorption bands in pure PVA and PVA/KCl films.

Samples	Wavenumbers of the minima (cm^{-1})	Extent of the minima shift (cm^{-1})
Pure PVA	3270	
PK0.25	3280	10
PK0.5	3288	18
PK0.75	3300	30
PK1	3306	36
PK3	3314	44
PK5	3330	60

CC BY

shift toward higher values can be highlighted by the shift of the minima of the hydroxyl absorption bands, as stated in Table 3.

As this shift suggests changes in hydrogen bonding among PVA chains, the higher the KCl nanoparticles content, the more the hydrogen bond structure is affected, indicating an enhancement of KCl–PVA interactions. This finding is further supported by the predicted occurrence of electrostatic attractions and coordination effects between K^+, Cl^- ions, and the polar groups of PVA chains during the elaboration process (solution casting method). Indeed, the water clusters $[K^+(H_2O)_5Cl^-]$, arising from the aqueous dissociation of KCl nanoparticles, undergo electrostatic interactions with the polar OH and CO groups of PVA, which can lead to the formation of other clusters and coordination complexes, disturbing the hydrogen bond structure.

In the same context, it is recognised that halide ions (Cl^- in our case) act as proton acceptors and can make hydrogen bonds with hydroxyl groups [41]. As a result, the addition of KCl nanoparticles to PVA breaks some hydrogen bonds between OH groups of PVA chains (OH···OH) and forms new ones between Cl^- and hydroxyl groups (OH···Cl). The newly formed hydrogen bonds are weaker than those among PVA chains. So, the strength of O–H bonds in the presence of KCl nanoparticles becomes effectively stronger, causing a blue shift in the hydroxyl group absorptions in PVA/KCl films. About the K^+ cation, it acts as a proton donor and forms electrostatic interactions with water molecules via the non-bonding electron pairs of oxygen atoms. The subsequent weakening of the hydroxyl bonds causes a decrease in their vibration frequency. But this effect is dominated by the stronger influence of the Cl^- anion on the hydroxyl vibration frequency [42]. Consequently, the absorption bands ascribed to the O–H stretching vibration of hydroxyl groups are highly sensitive to the hydrogen bond structure. As the absorption intensity is proportional to the concentration of absorbing sites, the blue shift of the minima is associated with a transition of the maximum concentrations of absorbing sites toward those with higher vibrational frequency.

The other bands

The broad absorption band between 964 and 1166 cm^{-1} in the spectrum of pure PVA contains a narrow peak at 1145 cm^{-1} superimposed on a broader peak with a minimum around 1086 cm^{-1}. The first peak is attributed to CO stretching in the crystalline region [43], while the second corresponds to CO stretching and OH bending in the amorphous region of PVA [40,44]. The broadening of the latter peak explains the presence of multiple types of OH and CO bonds with varying lengths and strengths. It can be noted (Fig. 3) that the FT-IR spectra of PVA/KCl films display the same broad band of pure PVA. However, the relevant emergent fact is the increase in absorption intensities in the 1018–1085 cm^{-1} wavenumber region when the KCl nanoparticles content exceeds 10.1 %. Since absorptions in this frequency range originate from the amorphous region in PVA, it is reasonable to expect the same in PVA/KCl films. Consequently, the increase in absorption intensities likely reflects the increase of the amorphous fraction in the PK1, PK3 and PK5 films, as pointed by the decrease in the fraction of the crystalline region observed in the thermal properties (section 3.1). Other significant changes include the enhancement of peak intensities at 1720 and 1250 cm^{-1}, observed only for films with KCl nanoparticles content equal to or greater than 13 %, corresponding to C=O stretching and C–O bending, respectively. These peaks may be associated with residual acetate groups in PVA [44,45]. The increase of their intensities can furthermore correlate with the increase of the amorphous fraction, as this region is primarily affected by the addition of KCl nanoparticles [42]. Moreover, the growth of these peaks may result from interactions between K^+ and Cl^- ions and the polar CO groups of PVA, which are facilitated by the expansion of the amorphous region.

It is essential to note that the presence of water in all the films is confirmed by the peak at around 1650 cm^{-1}, attributed to water deformation and combination. However, it is recognized that adding KCl to PVA promotes water retention via K^+, Cl^- ions and water dipole interactions. At low and medium KCl nanoparticle concentrations, these increases the film's water content, while at high concentrations, a salting–out effect can limit or reduce this retention. Then, water concentration increases with KCl content. For KCl below 13 %, this explains the enhanced plasticizing effect of water, responsible for the decrease in T_{g1} (Table 2). For higher KCl nanoparticles content, water retention reduces the amount of free water, decreasing crystallinity. The salting-out effect may

CC BY

also account for the higher water evaporation peaks observed in the first heating scan (Fig. 2a).

Furthermore, the absence of additional peaks associated with KCl salt in the spectra of all PVA/KCl films is predictable, as this salt is commonly used due to its high optical transmittance [46,47]. Indeed, the ionic nature of KCl restricts its absorption spectrum to low wavenumber [48,49]. Consequently, any possible agglomeration or reassociation of K^+, Cl^- ions in PVA/KCl films is not detected by FT-IR analysis.

The vibrational analysis of PVA/KCl films clearly indicates that the polar groups on the PVA backbone facilitate the dissolution process of the KCl nanoparticles. Indeed, weak electrostatic interactions are generated between the polar groups and the dissociated cations and anions, which typically occur in the amorphous regions. As a result, the salt ions are successfully dissolved within the PVA chains, inducing a modification of the chemical functionalities.

Surface morphology

Film surface imaging using SEM

Scanning electron microscopy is a powerful tool for imaging sample surfaces using a focused

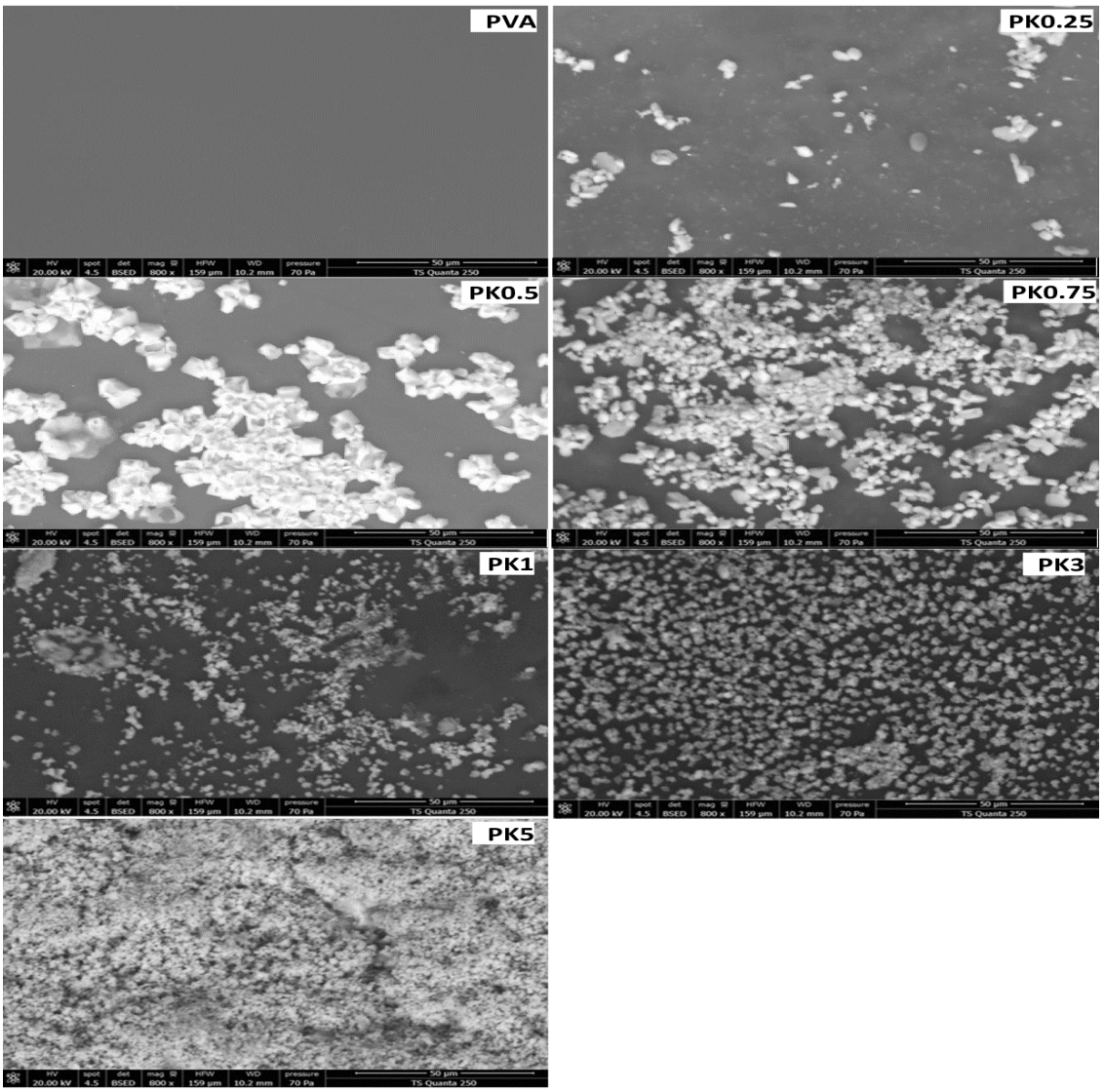


Fig. 4. SEM micrographs of the surfaces of the as-elaborated pure PVA and PVA/KCl films.

electron beam. This technique enables the assessment of the degree of compatibility, dispersion, and interaction between the sample components, which govern material properties (thermal conductivity, mechanical properties, optical properties,). The SEM micrographs recorded at room temperature for the surfaces of the as−elaborated pure PVA and PVA/KCl films are presented in Fig. 4.

Pure PVA film clearly exhibits a uniform surface morphology, indicating a homogeneous structure, a dense material, and a smooth surface. It can be observed that the addition of KCl nanoparticles to PVA results in a brighter background in the SEM micrographs compared to that of pure PVA. This brightness originates from the K^+ and Cl^- ions bonded to the hydroxyl groups of PVA and subsequently dissolved within the host matrix (section 3.2). The most striking effect is the appearance of brighter micrometric entities in the micrographs, even at low KCl contents (3.6 %). These entities rapidly grow with the addition of KCl, undergo agglomeration, and progressively cover a larger portion of the film surfaces. They appear as solid protrusions emerging from the surface. A closer examination of these agglomerated entities (PK0.5) shows an inhomogeneous brightness distribution. The brighter regions most likely correspond to microcrystalline aggregates of KCl nanoparticles formed at the film surface. The incapability of KCl salt to fully dissolve in the PVA matrix induces the pairing of the K^+ and Cl^- ions and their subsequent recrystallisation at the surface. At very low KCl nanoparticles content (3.6 %), microcrystals may originate from ion pairing within the aqueous mixture and migrate toward the surface during film drying. Indeed, in an aqueous KCl solution, 10 to 20 % of the ions undergo pairing [50]. The less bright areas may correspond to regions containing elements associated with the KCl salt. As the surface of KCl is known to be sensitive to humidity [22,51], the formed microcrystals may absorb water vapor from the surrounding atmosphere. Furthermore, as pointed out in Section 3.1, the evaporation of water from the aqueous mixture generates increasing competition for water molecules between salt ions and the hydroxyl groups of PVA. As a result, during drying at room conditions, undissolved K^+ and Cl^- ions in the PVA chains tend to bond with water molecules, due to their strong hygroscopic behaviour, and subsequently diffuse toward the film surface. The hydrated KCl salt then agglomerates, progressively swelling

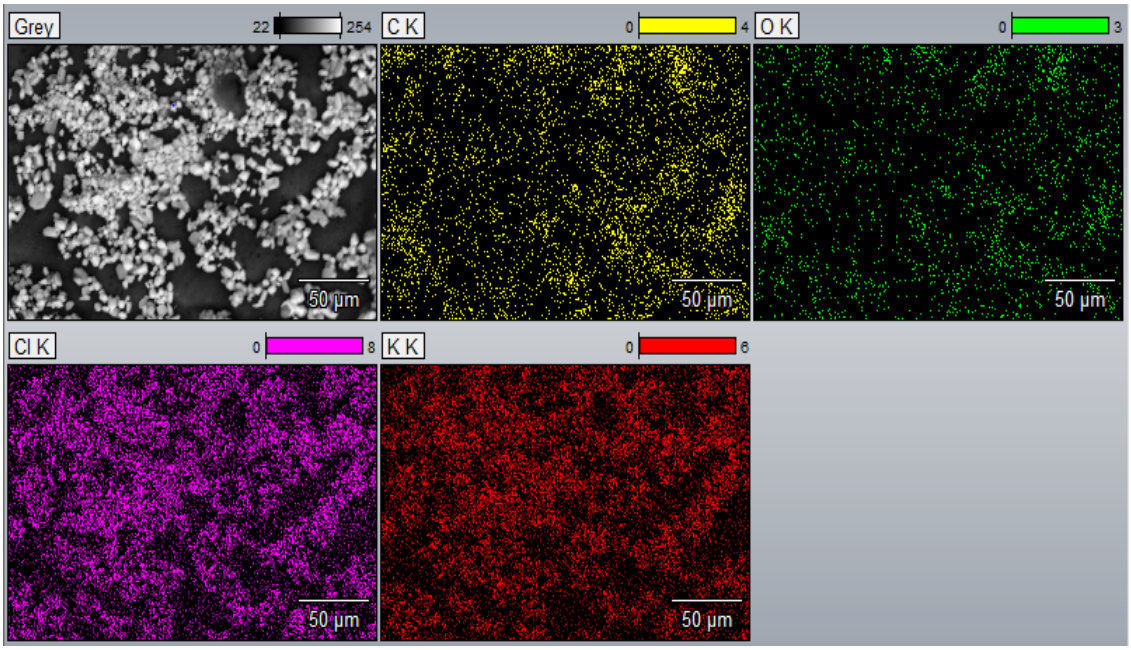


Fig. 5. EDX mapping images of carbon, oxygen, chlorine, and potassium elements on the PK0.75 surface. The first image, shown in grayscale, represents the SEM micrograph of the analysed surface.

CC BY

the film surface (PK1, PK3). At higher KCl contents (42.7 %), the SEM micrograph reveals a notable morphological transition. Indeed, the surface gets rougher and more porous, indicating the initiation of structural growing of hydrated KCl.

Energy Dispersive X−ray (EDX) mapping

It is well established that EDX mapping reveals details in SEM micrographs that are otherwise imperceptible, such as the spatial distribution and relative abundance of each element present on the film surface. For these purposes, and to further characterize the morphological transition indicated by the SEM micrographs, Fig. 5 displays the mapping images of carbon, oxygen, chlorine, and potassium elements at the surface of the PK0.75 film. The X−ray signal originates from the atom's inner K−shell transition, indicated in the mapped image by the letter "K" to the right of the element symbol. In addition, the element concentration at each point on the surface is represented by the highlighted bright dots.

It can be seen that carbon is more abundant than oxygen. Referring to their scaled concentrations, the ratio of their maximum concentration is 4/3. If these elements originated only from PVA chains, this ratio would be 2, as each monomer contains two carbon atoms and one oxygen atom. Nevertheless, oxygen also originates from water molecules bonded to PVA and from KCl nanoparticles. Then, the 4/3 ratio suggests that the maximum amount of oxygen from water is equal to that coming from PVA chains. As a result, this assessment of relative abundance provides a basis for the quantitative analysis of surface elements. Further examination of the EDX mapping image of carbon shows that this element is absent in regions of particle agglomeration. However, the higher concentrations are associated with the PVA matrix. Regarding the chlorine and potassium elements, they occupy the same spatial position, indicating their mutual attendance. Their spatial distribution displays two configurations: the first shows higher concentrations at the positions of microcrystal aggregates, while the second shows lower concentrations in the PVA matrix of the film surface, originating from K^+ and Cl^- ions dissolved within the PVA chains. Consequently, the EDX mapping images support the above attribution of microcrystals appearing on the surface to recrystallized KCl salt observed in the SEM micrographs. Furthermore, referring to the scaled concentrations, a higher abundance of chlorine is noted at the surface, which might result from partial hidden of K^+ ions by water molecules, as this cation is more hydrophilic than Cl^- [50,51]. The examination of SEM micrographs and EDX mapping images clearly proves an intriguing behavior of KCl nanoparticles in PVA/KCl films. Indeed, even with the good dissociation ability of the host PVA, undissolved K^+ and Cl^- ions attract water molecules and diffuse to the surface during film drying. Evidently, this phenomenon increases with the addition of KCl nanoparticles and, beyond a certain threshold, can break the growth of film crystallinity. The diffusion of hydrated KCl toward the surface limits the remaining amount of water beneath the surface. Consequently, the mobility of the PVA chains is reduced, which halts crystallization rapidly. This explanation aligns with the observed decrease in the crystallinity fraction for films containing more than 10.1 % KCl.

Conductivity analysis

In this section, pure PVA and PVA/KCl films were characterized by impedance spectroscopy to highlight the correlation between their structure and conductivity mechanism. Indeed, impedance spectroscopy is a well−recognized method for characterizing ion conduction in polymers and their frequency and temperature−dependent behaviour.

General consideration

The complex alternating current (AC) conductivity σ^*_{AC} was determined from the complex impedance $Z^*(\omega)=Z'(\omega)+jZ''(\omega)$ using the relation:

$$\sigma^*_{AC}(\omega) = \frac{d}{A\,Z^*} = \frac{d}{A}\left[\frac{Z'}{(Z')^2+(Z'')^2} - j\,\frac{Z''}{(Z')^2+(Z'')^2}\right] = \sigma'_{AC}(\omega) - j\,\sigma''_{AC}(\omega) \quad (1)$$

where ω denotes the angular frequency ($\omega=2\pi F$), j is the imaginary unit ($j^2=-1$), and d and A represent the thickness and the surface area of the film, respectively. The real part of the AC conductivity $\sigma\rangle_{AC}$ corresponds to the dissipative or resistive response of the material and hence its energy loss. While the imaginary part $\sigma\rangle\rangle_{AC}$ reflects its reactive or inductive response and thus its energy storage. Optimizing material performance across all electrical domains requires

CC BY

precise knowledge of its dissipative conductivity. Consequently, this important parameter will be considered in the conductivity analysis of the prepared films. The curves showing the variations of the real part of AC conductivity $\sigma\rangle_{AC}$ versus frequency for pure PVA and PVA/KCl films at ambient temperature (T_a) are presented in Fig. 6. This variation can be classified into three frequency domains. In the intermediate region, the conductivity exhibits frequency–independent behaviour with an almost constant value, representing the direct current (DC) conductivity, σ_{DC}. At high frequency, the conductivity increases with frequency following a power–law behavior. At low frequency, an additional frequency–dependent conductivity region appears before the plateau, displaying a drop–in conductivity. This phenomenon, known as electrode polarization (EP), is an experimental artefact attributed to the blocking of charge carriers at the interface between the electrode and the film surface [52,53]. The Jonscher's universal relation can express the main conductivity variations:

$$\sigma'_{AC}(\omega, T) = \sigma_{DC}(T) + A(T)\,\omega^{s(\omega,T)} \quad (2)$$

where T is the absolute temperature, A is a temperature-dependent proportionality coefficient, and s is the exponent of the power law, ranging between 0 and 1.

It is recognized that the DC conductivity σ_{DC} depends on the movement of free charge carriers through the polymer and is frequency–independent. However, the AC conductivity is associated with localized charge carriers, which can undergo delocalization at high frequencies. As a result, σ_{DC} can be determined from the plateau region of the $\sigma\rangle_{AC}$ versus frequency curve [54]. For this reason, Jonscher's universal law is used to fit the conductivity measurements data, as illustrated by the solid lines in Figs. 6 and 7, to determine the values of σ_{DC} and the power–law exponent s.

Conductivity variation with KCl nanoparticles content at room temperature

The general trend shown by the curves in Fig. 6 is the enhancement of the real part of the AC conductivity with KCl nanoparticles content for films containing less than 13 %. Above this content, $\sigma\rangle_{AC}$ decreases, and for the PK5 film, it becomes even lower than that of pure PVA. The pure PVA film exhibits an almost frequency–dependent conductivity. The assessed value of σ_{DC} is approximately 1.8×10^{-12} S/cm, indicating

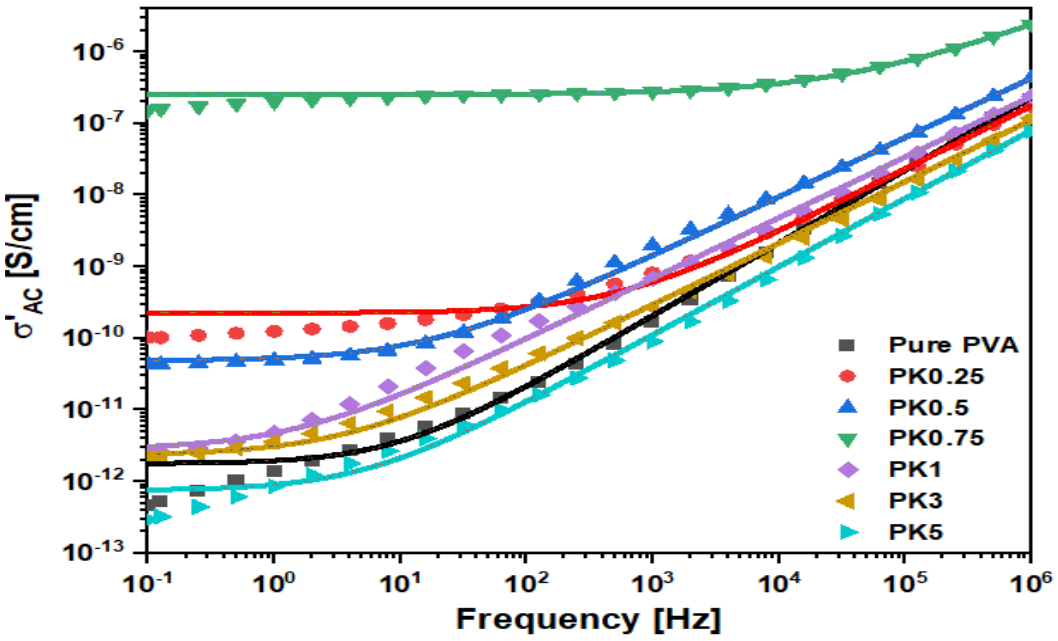


Fig. 6. Variations of the real part of AC conductivity $\sigma\rangle_{AC}$ versus frequency for pure PVA and PVA/KCl films at $T_a \approx 20$ °C. The solid lines represent the best-fitted curves according to Jonscher's relation.

CC BY

a lack of free charge carriers and making it a suitable insulating polymer for charge storage and insulation in electronic applications. The low DC conductivity of PVA is attributed to its molecular structure, consisting of long chains of carbon atoms covalently bonded to hydrogen and oxygen atoms. Its polar hydroxyl groups form strong hydrogen bonds with each other, with neighbouring chains, and even with absorbed water molecules, resulting in a rigid and firmly bound polymer. Furthermore,

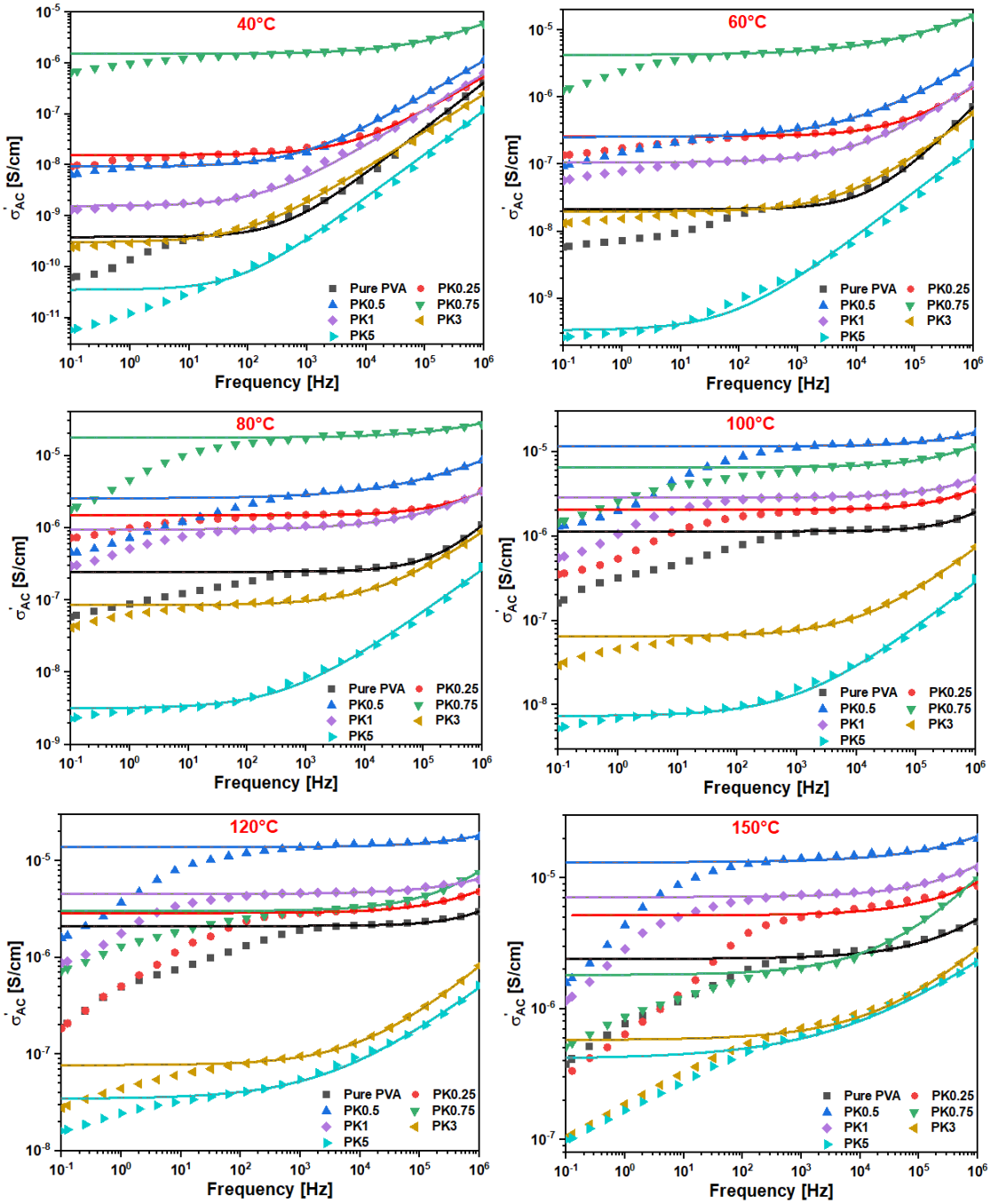


Fig. 7. Variations of σ›$_{AC}$ with frequency for pure PVA and PVA/KCl films at the corresponding temperatures. The solid lines represent the best-fitted curves to Jonscher's relation.

CC BY

even if PVA contains ionic impurities originating from its manufacturing process, these impurities are fixed within the polymer chains. In addition, the restriction flexibility and segmental motion of PVA chains are also attributed to their glassy state nature, as T_a is lower than $T_{g1} \approx 39°C$. An intriguing behaviour is observed for the PK0.75 film. Indeed, its higher DC conductivity, approximately 2.5×10^{-7} S/cm, is more than five orders of magnitude greater than that of pure PVA and remains almost frequency-independent up to 10^4 Hz. This conductivity enhancement is far greater than the stated only one order of magnitude [22,23]. As a result, the elaborated film with 10.1 % KCl, prepared using the casting method, exhibits higher DC conductivity that is frequency–independent over a wide range of frequencies at ambient temperature. Consequently, this film represents a promising candidate for several specific applications.

The above variation of DC conductivity with KCl nanoparticles content aligns with the results of FT-IR analysis and surface morphology, both performed at room temperature, T_a. A common observation is the clear difference on either side of 13 % KCl. At low KCl nanoparticle contents, the enhancement in σ_{DC} with KCl concentration is associated with an increase in the density and mobility of free charge carriers, correlated with the greater amount of nanoparticles added during film elaboration. As noted above, the addition of KCl salt to PVA breaks some hydrogen bonds among the OH groups of PVA chains (OH···OH) and forms new ones (OH···Cl) with Cl^- (proton acceptors) inducing the release of water, while K^+ binds with water molecules (proton donors). Consequently, the predictable increase in these interactions with KCl content raises the density of charge carriers K^+, Cl^-, H^+ and OH^- arising from KCl salt and released water molecules. It provides an additional pathway through PVA chains, bolstering ionic conductivity within the films. This enhancement of DC conductivity reaches its maximum at 10.1 % KCl nanoparticles.

For KCl content higher than 10.1 %, the decrease in conductivity is unexpected, as the fraction of amorphous phases increases with KCl content (Table 2 and $T_a > T_{g1} \approx 17°C$). Indeed, it is reasonable to assume that a large amorphous phase provides continuous pathways for ion movement, thereby enhancing conductivity. The observed decrease in conductivity could be attributed to the pairing of K^+ and Cl^- ions and their extensive clustering at high KCl nanoparticle concentrations, resulting in the formation of neutral species that reduce the density and mobility of free ions. FT-IR results have revealed the emergence of additional absorption peaks in the spectra, attributed to the possible growth of interactions between K^+ and Cl^- ions and the polar CO groups of the PVA chains. However, it would normally be expected to enhance ionic conductivity, as is the case with the hydroxyl groups of PVA. SEM micrographs reveal the formation of KCl microcrystals and the structural growth of hydrated KCl at the film surface, limiting the remaining amount of released water beneath the surface. This can explain the decrease on conductivity of PVA/KCl films with the addition of KCl nanoparticles. Furthermore, this morphological modification of the film surface likely behaves as an insulating layer, reducing the film's conductivity. Indeed, solid KCl is recognized as an insulating material due to its strong ionic bond, and the water molecules in hydrated KCl are incorporated into the crystal structure while preserving these ionic bonds.

Thermal activation of conductivity

Impedance measurements of the films were performed in the temperature range of 20 - 150°C and over a frequency range between 10^{-1} and 10^6 Hz. The real part of AC conductivity was calculated using Eq. (1). The curves showing the variations of σ_{AC} with frequency for all films at relevant temperatures are presented in Fig. 7.

As expected, thermally activated conductivity

Table 4. DC conductivity values (in S/cm) at different temperatures for pure PVA and PVA/KCl films.

T(°C)	20	40	60	80	100	120	150
PVA	1.8×10^{-12}	3.8×10^{-10}	2.2×10^{-8}	2.5×10^{-7}	1.1×10^{-6}	2.1×10^{-6}	2.4×10^{-6}
PK0.25	2.3×10^{-10}	1.6×10^{-8}	2.6×10^{-7}	1.5×10^{-6}	2×10^{-6}	2.9×10^{-6}	5.2×10^{-6}
PK0.5	4.9×10^{-11}	9.3×10^{-9}	2.5×10^{-7}	2.6×10^{-6}	1.2×10^{-5}	1.3×10^{-5}	1.3×10^{-5}
PK0.75	2.5×10^{-7}	1.5×10^{-6}	4.3×10^{-6}	1.8×10^{-5}	6.5×10^{-6}	3×10^{-6}	1.8×10^{-6}
PK1	2.8×10^{-12}	1.6×10^{-9}	1×10^{-7}	9.5×10^{-7}	2.8×10^{-6}	4.5×10^{-6}	7.2×10^{-6}
PK3	2.4×10^{-12}	3×10^{-10}	2×10^{-8}	8.5×10^{-8}	6.5×10^{-8}	7.7×10^{-8}	5.8×10^{-7}
PK5	7.5×10^{-13}	6×10^{-11}	3.4×10^{-10}	3.2×10^{-9}	7.4×10^{-9}	3.5×10^{-8}	4.2×10^{-7}

CC BY

is observed. The main changes associated with increasing temperature are the expansion of the plateau region and its shift toward high frequencies. Consequently, the frequency dependent conductivity region shrinks, while the experimental artefact region expands. It is evident that as the temperature increases, an increasing number of localized charges undergo thermal delocalization, even at low frequencies. These delocalised charges become free carriers, thereby enhancing σ_{DC} instead of remaining confined to high−frequency delocalisation.

The values of σ_{DC} at different temperatures for pure PVA and PVA/KCl films are summarized in Table 4.

It can be noted that for pure PVA, the rate of increase in DC conductivity is greater between 20 and 60°C, but gradually decreases as the temperature rises further. This observation highlights a significant change in the conductive properties of PVA. Indeed, the temperature range between 20 and 60°C lays around the glass transition temperature T_{g1}≈39°C and highlights the transition from glassy to the rubbery states, which begins just above T_g1 and extends over a limited temperature interval. In the amorphous state, the flexibility and segmental motion of PVA chains are exclusively promoted, leading to the release of ionic impurities that enhance DC conductivity. These phenomena clearly persist above 60°C, where the increasing thermal agitation induces a higher degree of disorder in the PVA matrix, thereby limiting the rate of conductivity enhancement. It is also important to note that this variation in DC conductivity occurs concomitantly with water evaporation above room temperature (Fig. 2a), which likely contributes to the improvement of PVA conductivity. Indeed, water molecules are initially bonded to the hydroxyl groups of PVA chains at room temperature and undergo thermal bond breaking before they can evaporate. The released molecules increase the flexibility and segmental motion of the PVA chains by enlarging the free volume, and they may also dissociate into H^+ and OH^- ions, thus enhancing conductivity. As the temperature continues to rise, a competition emerges between the release of water molecules and their evaporation, which could explain the deceleration in the growth rate of conductivity. Indeed, above 60°C, the accelerated evaporation of water likely restricts the segmental mobility of PVA chains, thereby slowing down the increase in conductivity.

The effect of increasing temperature on the

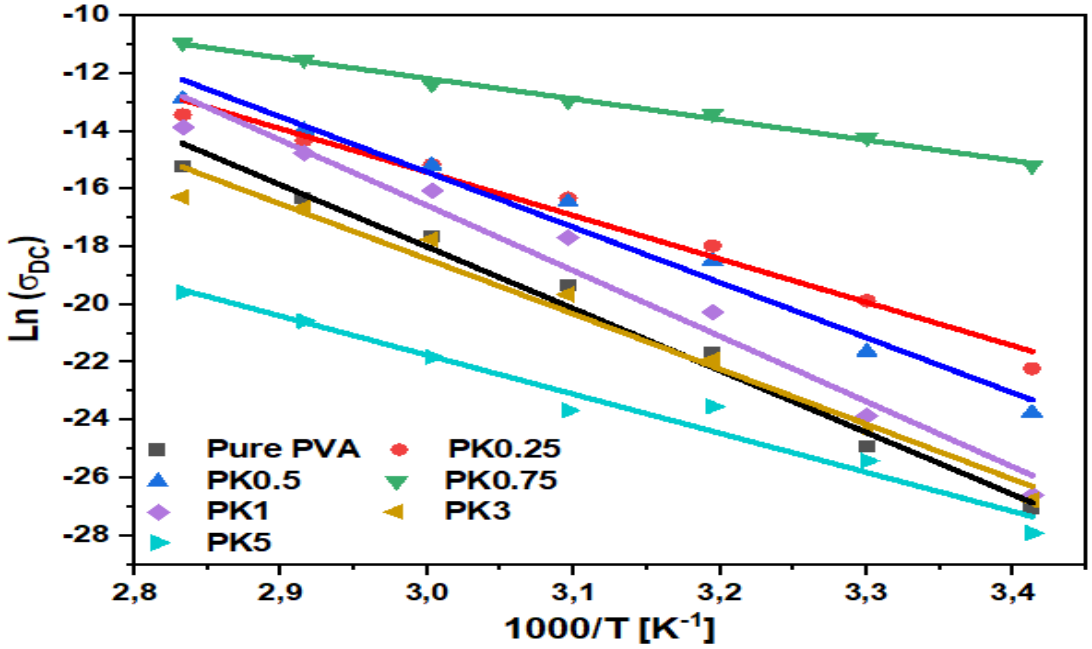


Fig. 8. Logarithmic variation of DC conductivity with 1000/T for the pure PVA and PVA/KCl films. The solid lines represent the best-fitted curves according to the Arrhenius model.

conductivity of PVA/KCl films is globally similar to that of pure PVA, regardless of the KCl nanoparticles content (Fig. 7 and Table 4). Furthermore, the trend of DC conductivity variation with KCl content observed at room temperature is maintained up to 80°C. In particular, films containing less than 13 % KCl display the highest conductivity. The σ_{DC} values of the PK0.75 film are the highest, reaching approximately 1.8×10^{-5} S/cm at 80°C. However, their rate of DC conductivity increase indicates greater thermal stability, which is crucial for certain technological applications. Above 80°C, the most notable effect is a slight decrease of σ_{DC} for the PK0.75 film, whereas the σ_{DC} of PK0.5 continues to increase, reaching a maximum of approximately 1.3×10^{-5} S/cm at 110°C, which is maintained up to 150°C. For films containing more than 10.1 % KCl, their σ_DC at room temperature is close to that of pure PVA. As the temperature increases, σ_{DC} grows, reaching values comparable to those of PK0.75 at 20°C and pure PVA at 150°C. Consequently, blinding PVA with more than 10.1 % KCl nanoparticles does not significantly enhance the film conductivity.

It is well established that the growth of DC conductivity with temperature is due to the rise in the number of free mobile carriers and their mobility. As pointed out above, the temperature increase is associated with enhanced flexibility and segmental motion of the PVA chains. Consequently, the fraction of free volume increases, facilitating the transient motion of K^+ and Cl^- ions and providing additional pathways for ion transport. Furthermore, the temperature rise promotes the dissociation of weaker bonds created by the addition of KCl nanoparticles, such as those between hydroxyl groups and Cl^- (proton acceptors) and between K^+ and water molecules (proton donors). These effects are also promoted by water release and evaporation. As a result, the density of free ions increases, and additional coordinated sites are generated, promoting the mobility of charge carriers within the films.

As pointed out above, PK0.5 and PK0.75 films exhibit different thermal variations in their conductivities at temperatures greater than or equal to 80°C. The slight decrease in DC conductivity of PK0.75 before reaching its maximum at 80°C indicates a reduction in the number of free ions or a decrease in their mobility. The PK0.5 film, on the other hand, reaches a thermally independent DC conductivity state at T ≥ 110°C, with a value close to its maximum. It is expected that the PK0.75 film contains more free ions than the PK0.5 due to the higher amount of added KCl nanoparticles. This explains the higher σ_{DC} values of PK0.75 up to 80°C, which are about one order of magnitude greater than those of PK0.5 at the same temperature. However, the decrease of σ_{DC} for PK0.75 by one order of magnitude between 80 and 150°C may indicate some pairing or clustering of K^+ and Cl^- ions at high nanoparticles content, or a slight reduction in free ions mobility, which is sensitive to material disorder, especially at higher temperatures. These blocking effects are expected to be less pronounced in PK0.5. As a result, the PK0.75 film is a suitable candidate for applications requiring temperatures below 100°C, whereas PK0.5 is more relevant for higher temperatures.

For films containing more than 10.1 % KCl

Table 5. Activation energy E_a and high-temperature DC conductivity σ_0 values for pure PVA and PVA/KCl films.

Films	σ_0 (S/cm)	E_a (eV)
Pure PVA	4.6×10^{19}	1.83
PK0.25	6.4×10^{15}	1.33
PK0.5	1.6×10^{18}	1.66
PK0.75	9.3×10^{3}	0.62
PK1	1.9×10^{22}	1.96
PK3	6.6×10^{16}	1.65
PK5	1.5×10^{8}	1.17

CC BY

nanoparticles, thermal activation does not significantly enhance their conductivity, as these films exhibit σ_{DC} values close to those of pure PVA at all temperatures. This explains the negligible contribution of both microcrystal and hydrated KCl to the film's conductivity. Indeed, the considered temperature range is too low to induce KCl dissociation in these structures.

For the purpose of characterising the thermal activation of the DC conductivity mechanism, the logarithmic variation of this conductivity with 1000/T was plotted for pure PVA and PVA/KCl films, as illustrated in Fig. 8.

The linear variation highlights a thermally activated mechanism according to the Arrhenius model:

$$\sigma_{DC} = \sigma_0 \exp\ (-E_a / K_B\ T) \quad (3)$$

where σ_0 is a pre-exponential factor representing the DC conductivity at high temperature, E_a is the activation energy, K_B is the Boltzmann constant, and T is the absolute temperature (K). The calculated values of E_a and σ_0 are summarized in Table 5. It can be observed that a high value of E_a is associated with a high σ_0. This indicates that a mechanism with high activation energy requires more thermal energy to proceed. Consequently, the main increase in conductivity occurs at higher temperature ($T \gg E_a/K_B$), if the same mechanism is involved, resulting in a high σ_0 value.

The pure PVA film exhibits a high activation energy of approximately 1.83 eV, which is higher than the value of 1.495 eV reported in our previous work using a different PVA powder with a lower molecular weight (ranging from 85 000 to 124 000 g/mol) [26]. This shift is consistent with the growth of E_a with molecular weight. The high E_a in PVA reflects the energy spent to enhance the flexibility and segmental motion of PVA chains. The PK0.75 film, which exhibits the highest conductivity, has the lowest activation energy, a desirable property for practical applications. This means that charge carriers require less energy to become free and move within highly conducting films. The decrease of E_a with increasing KCl content for PK1, PK3, and PK5 can be explained by the expansion of their amorphous region. Indeed, in these regions, ion motion is facilitated throughout the film network.

It is well known that DC conductivity is proportional to the density of free charge carriers and their mobility. As both are thermally activated, the assessed activation energy E_a reflects their combined contribution. The activation energy associated with the density of free charge carriers corresponds to the energy spent for their release. Indeed, ions are bonded to PVA chains or water molecules and must be freed as the temperature increases. The mobility of charge carriers and their thermal activation in disordered materials is a complex phenomenon. However, it is reasonable to assume that the thermal activation of the vibrational motion of the PVA backbone and side chains brings the transit sites closer together, creating pathways that facilitate ion movement.

CONCLUSION

The thermal, vibrational, surface morphological, and conductive properties of pure PVA and PVA blended with various weight fractions of KCl nanoparticles (ranging from 3.6 % to 42.7 %) elaborated via the solution casting method, were investigated. DSC analysis revealed higher glass transition temperatures after water evaporation and a drastic reduction in crystallinity, along with overlapping water evaporation peaks, for films containing more than 10.1 % KCl. FT-IR spectra showed a progressive blue shift of the hydroxyl absorption band as the KCl content increased, confirming the interaction of K^+ and Cl^- ions within the PVA matrix. For KCl contents above 10.1 %, the enhancement of specific absorption band intensities was attributed to the increase of the amorphous fraction. In the same composition range, SEM micrographs and EDX mapping revealed the formation of hydrated KCl crystals and microcrystals, indicating that the hygroscopic nature of KCl enables the undissolved K^+ and Cl^- ions to attract water molecules and diffuse to the surface during film drying. Conductivity analysis revealed that the AC conductivity strongly depends on KCl nanoparticles content, frequency, and temperature. The DC conductivity increased with KCl content up to 10.1 %, reaching 2.5×10^{-7} S/cm at 20 °C, representing an enhancement of five orders of magnitude compared to pure PVA. Beyond this concentration, further addition of KCl did not significantly improve conductivity. The film containing 10.1 % KCl is thus suitable for applications operating below 100°C, whereas the one containing 6.9 % KCl performs better at higher temperatures. The thermally activated DC conductivity followed the Arrhenius model, with activation energies ranging from 0.62 to

CC BY

1.96 eV. Overall, blending PVA with 6.9 – 10.1 % KCl nanoparticles effectively enhances ionic conduction in PVA films, offering low cost, biodegradable and promising prospects for flexible electronics and energy storage applications.

CONFLICT OF INTEREST

The authors declare that there is no conflict of interests regarding the publication of this manuscript.

REFERENCES

1. Rambabu SL, Arulsankar A, Jeya S, Christopher Jeyaseelan S, Sundaresan B, Sakthipandi K. Structural and electrical studies of ultra-sonicated sodium-ion embedded polyvinyl alcohol and polyvinyl pyrrolidone solid polymer blend electrolytes. J Indian Chem Soc. 2025;102(11):102138.
2. Hamsan MH, Aziz SB, Azha MAS, Azli AA, Shukur MF, Yusof YM, et al. Solid-state double layer capacitors and protonic cell fabricated with dextran from Leuconostoc mesenteroides based green polymer electrolyte. Materials Chemistry and Physics. 2020;241:122290.
3. Fahad OA, Mohammed AS, Salih EY, Mohammed MKA. Perpendicular sheet-like alignment of a self-driven MoS_2 /Si heterostructure for Vis-NIR wavelength detection. Nanoscale. 2025;17(30):17795-17802.
4. Kumar G, Singh R, Chand P, Kumar M, Singh RR, Kumar A. A review on polymer electrolyte materials in context to modifications in PVDF-HFP polymer host. J Solid State Electrochem. 2025;29(11):4493-4528.
5. Altaf M, Maurya JC, Haldar AK, Demirci UB. A systematic review of the last three decades on magnesium-based polymer composites for solid-state hydrogen storage. Int J Hydrogen Energy. 2026;205:153314.
6. Jayanthi S, Rajamani D. Development of solid polymer electrolytes using PMMA, Lithium nitrate, and Nanosilica for battery applications. Materials Science and Engineering: B. 2026;324:118996.
7. Abed.Fahad O, Hanfoosh SM, Mohammed AS. High-Performance Visible-Light Photodetectors Based on CeO_2-Doped V2O5 Nanostructure: Optoelectronic Characterization. Plasmonics. 2025;20(12):11255-11264.
8. Yao Y, Hsu Y-I, Uyama H. Enhanced physical properties and water resistance of films using modified starch blend with poly(vinyl alcohol). Industrial Crops and Products. 2024;222:119870.
9. Gond DK, Satyarthi SK, Vandna, Yadav BK, Upadhyay SN, Mishra PK, et al. Alkali-treated PVA/flax fiber biocomposite films for sustainable packaging applications. J Indian Chem Soc. 2026;103(9):102896.
10. Hdidar M, Chaari M, Haddar N, Megdiche M, Arous M. Synthesis and characterization of polyvinyl alcohol crosslinked with various degrees of oxalic acid for advanced ionic conductive applications. Ionics. 2025;31(6):5611-5626.
11. Alshikeewi SAM, Hdidar M, Megdiche M, Arous M. Effect of copper and vanadium oxide doping on the electrical and impedance behavior of PVA nanocomposite films. Euro-Mediterranean Journal for Environmental Integration. 2026;11(5).
12. Alanazi HT. Synergistic enhancement of optical and electrical performance in CMC/PVP nanocomposites via NiO/$NiFe_2O_4$ hybrid nanofillers. Ceram Int. 2026;52(20):36786-36796.
13. Georgieva N, Bryaskova R, Tzoneva R. New Polyvinyl alcohol-based hybrid materials for biomedical application. Mater Lett. 2012;88:19-22.
14. Chae JS, Heo N-S, Kwak CH, Cho W-S, Seol GH, Yoon W-S, et al. A biocompatible implant electrode capable of operating in body fluids for energy storage devices. Nano Energy. 2017;34:86-92.
15. Teodorescu M, Bercea M, Morariu S. Biomaterials of PVA and PVP in medical and pharmaceutical applications: Perspectives and challenges. Biotechnol Adv. 2019;37(1):109-131.
16. Nugrahani Primary Putri II. Synthesis and Characterization of PANi/PVA Nanofibers with Variation of Nozzle to Collector Distance Using Electrospinning Method. Indonesian Physical Review. 2022;5(3):137-147.
17. Saroj AL, Singh RK. Thermal, dielectric and conductivity studies on PVA/Ionic liquid [EMIM][EtSO4] based polymer electrolytes. Journal of Physics and Chemistry of Solids. 2012;73(2):162-168.
18. Yong J, Chen Y-C, Aziz SB, Khandaker MU, Woo HJ. Correlated barrier hopping dynamics of Na+ ions in poly(vinyl alcohol) biopolymer-based solid polymer electrolytes: Electrical and structural analysis. Electrochimica Acta. 2025;513:145610.
19. Org Mass Spectrom. 1984;19(10).
20. Zhu X, Ali RN, Song M, Tang Y, Fan Z. Recent Advances in Polymers for Potassium Ion Batteries. Polymers. 2022;14(24):5538.
21. Freney EJ, Martin ST, Buseck PR. Deliquescence and Efflorescence of Potassium Salts Relevant to Biomass-Burning Aerosol Particles. Aerosol Sci Technol. 2009;43(8):799-807.
22. Jing B, Peng C, Wang Y, Liu Q, Tong S, Zhang Y, et al. Hygroscopic properties of potassium chloride and its internal mixtures with organic compounds relevant to biomass burning aerosol particles. Sci Rep. 2017;7(1).
23. Solangi MY, Aftab U, Ishaque M, Bhutto A, Nafady A, Ibupoto ZH. Polyvinyl fibers as outperform candidature in the solid polymer electrolytes. J Ind Text. 2020;51(4_suppl):6983S-6995S.
24. Pavani Y, Ravi M, Bhavani S, Sharma AK, Narasimha Rao VVR. Characterization of poly(vinyl alcohol)/potassium chloride polymer electrolytes for electrochemical cell applications. Polymer Engineering and Science. 2012;52(8):1685-1692.
25. Liu Y, Vrana NE, Cahill PA, McGuinness GB. Physically crosslinked composite hydrogels of PVA with natural macromolecules: Structure, mechanical properties, and endothelial cell compatibility. Journal of Biomedical Materials Research Part B: Applied Biomaterials. 2009;90B(2):492-502.
26. Hdidar M, Chouikhi S, Fattoum A, Arous M. Effect of hydrolysis degree and mass molecular weight on the structure and properties of PVA films. Ionics. 2017;23(11):3125-3135.
27. Hodge RM, Edward GH, Simon GP. Water absorption and states of water in semicrystalline poly(vinyl alcohol) films. Polymer. 1996;37(8):1371-1376.
28. Harper JF. Mechanics of Engineering Materials. P. P. Benham and R. J. Crawford. Longman Scientific and Technical, Harlow. 1987. 626pp. Illustrated. £15.95. Mechanics of Engineering Materials: Solutions Manual, P. P. Benham and

CC BY

R. J. Crawford. Longman Scientific and Technical, Harlow. 1987. 289 pp. Illustrated. £9.95. The Aeronautical Journal. 1988;92(915):203-203.
29. Lue SJ, Shieh S-J. Modeling water states in polyvinyl alcohol-fumed silica nano-composites. Polymer. 2009;50(2):654-661.
30. Max J-J, Chapados C. Infrared spectra of cesium chloride aqueous solutions. The Journal of Chemical Physics. 2000;113(16):6803-6814.
31. Max J-J, Chapados C. IR spectroscopy of aqueous alkali halide solutions: Pure salt-solvated water spectra and hydration numbers. The Journal of Chemical Physics. 2001;115(6):2664-2675.
32. Sen A, Ganguly B. What is the minimum number of water molecules required to dissolve a potassium chloride molecule? J Comput Chem. 2010;31(16):2948-2954.
33. Hamid NM, Abed HA, Fahad OA. Evaluation of Antibacterial Effects of Silver Nanoparticles Synthesized via Pulsed Laser Ablation at Different Laser Energies. Lasers in Manufacturing and Materials Processing. 2025;12(3):488-497.
34. Hassen A, El Sayed AM, Morsi WM, El-Sayed S. Influence of Cr_2O_3 nanoparticles on the physical properties of polyvinyl alcohol. J Appl Phys. 2012;112(9).
35. Kozlov M, McCarthy TJ. Adsorption of Poly(Vinyl Alcohol) from Water to a Hydrophobic Surface: Effects of Molecular Weight, Degree of Hydrolysis, Salt, and Temperature. Langmuir. 2004;20(21):9170-9176.
36. Abdel-Baset TA, Hassen A. Dielectric relaxation analysis and Ac conductivity of polyvinyl alcohol/polyacrylonitrile film. Physica B: Condensed Matter. 2016;499:24-28.
37. Aziz SB, Abidin ZHZ. Electrical Conduction Mechanism in Solid Polymer Electrolytes: New Concepts to Arrhenius Equation. Journal of Soft Matter. 2013;2013:1-8.
38. Bhagavannarayana G, Parthiban S, Meenakshisundaram S. An Interesting Correlation between Crystalline Perfection and Second Harmonic Generation Efficiency on KCl- and Oxalic Acid-Doped ADP Crystals. Crystal Growth and Design. 2007;8(2):446-451.
39. Suresh N, Selvapandiyan M. Influence of Zirconium Nitrate doping on the properties of l-Alanine crystal for nonlinear optical applications. Journal of Materials Science: Materials in Electronics. 2020;31(19):16737-16745.
40. Xiao S, Gao R, Gao L, Li J. Poly(vinyl alcohol) films reinforced with nanofibrillated cellulose (NFC) isolated from corn husk by high intensity ultrasonication. Carbohydr Polym. 2016;136:1027-1034.
41. Allerhand A, von Rague Schleyer P. Halide Anions as Proton Acceptors in Hydrogen Bonding. Journal of the American Chemical Society. 1963;85(9):1233-1237.
42. Tretinnikov ON, Zagorskaya SA. Effect of alkali halide salt additives on the structure of poly(vinyl alcohol) films cast from aqueous solutions. Polymer Science Series A. 2013;55(8):463-470.
43. Tadokoro H. Structure and properties of crystalline polymers. Polymer. 1984;25(2):147-164.
44. Qua EH, Hornsby PR, Sharma HSS, Lyons G, McCall RD. Preparation and characterization of poly(vinyl alcohol) nanocomposites made from cellulose nanofibers. J Appl Polym Sci. 2009;113(4):2238-2247.
45. Fernández MD, Fernández MJ. Thermal degradation of copolymers from vinyl acetate and vinyl alcohol. J Therm Anal Calorim. 2008;92(3):829-837.
46. Li Y, Li Y, Meng F, Zhang X, Zeng F, Liu J, et al. Effect of cooling time on the structural, optical, mechanical, thermal and electrical properties of KCl1−xBrx crystals formed directly on cooling the melt. Journal of Materials Science: Materials in Electronics. 2021;32(11):15425-15440.
47. Solgi S, Samavat F, Mirzakuchaki S, Sasani Ghamsari M. Effect of different type of dopants on the enhancement of KCl single crystal optical properties. Optik. 2021;241:166554.
48. Ram RS, Dulick M, Guo B, Zhang KQ, Bernath PF. Fourier Transform Infrared Emission Spectroscopy of NaCl and KCl. Journal of Molecular Spectroscopy. 1997;183(2):360-373.
49. Barton EJ, Chiu C, Golpayegani S, Yurchenko SN, Tennyson J, Frohman DJ, et al. ExoMol molecular line lists V: the ro-vibrational spectra of NaCl and KCl. Mon Not R Astron Soc. 2014;442(2):1821-1829.
50. Soniat M, Pool G, Franklin L, Rick SW. Ion association in aqueous solution. Fluid Phase Equilib. 2016;407:31-38.
51. Li X, Gupta D, Eom H-J, Kim H, Ro C-U. Deliquescence and efflorescence behavior of individual NaCl and KCl mixture aerosol particles. Atmos Environ. 2014;82:36-43.
52. Khiar ASA, Arof AK. Conductivity studies of starch-based polymer electrolytes. Ionics. 2009;16(2):123-129.
53. Francis KMG, Subramanian S, Shunmugavel K, Naranappa V, Pandian SSM, Nadar SC. Lithium Ion-conducting Blend Polymer Electrolyte Based on PVA–PAN Doped with Lithium Nitrate. Polymer-Plastics Technology and Engineering. 2015;55(1):25-35.
54. Aziz SB, Abdullah OG, Rasheed MA. Structural and electrical characteristics of PVA:NaTf based solid polymer electrolytes: role of lattice energy of salts on electrical DC conductivity. Journal of Materials Science: Materials in Electronics. 2017;28(17):12873-12884.
55. Alipoori S, Aboutalebi SH, Barsbay M. Enhancing the performance of solid-state supercapacitors: Optimizing the molecular interactions in flexible gel polymer electrolytes. J Solid State Electrochem. 2024;28(8):2643-2657.